Journal of Pharmaceutical and Biomedical Analysis 197 (2021) 113947

Contents lists available at ScienceDirect

Journal of Pharmaceutical and Biomedical Analysis

journal homepage: www.elsevier.com/locate/jpba

Structural characterization of fondaparinux interaction with per-6-amino-beta-cyclodextrin: An NMR and MS study

Bianka Várnai[a], Márkó Grabarics[b,c], Zoltán Szakács[d], Kevin Pagel[b,c], Milo Malanga[e], Tamás Sohajda[e], Szabolcs Béni[a,*]

[a] Semmelweis University, Department of Pharmacognosy, Üllői út. 26, H-1085, Budapest, Hungary
[b] Freie Universität Berlin, Institute of Chemistry and Biochemistry, Arnimallee 22, 14195, Berlin, Germany
[c] Fritz Haber Institute of the Max Planck Society, Department of Molecular Physics, Faradayweg 4–6, 14195, Berlin, Germany
[d] Gedeon Richter Plc., Spectroscopic Research Department, H-1475, Budapest, P.O.B. 27, Hungary
[e] CycloLab, Cyclodextrin R&D Ltd, Budapest, H-1097, Illatos út 7, Hungary

ARTICLE INFO

Article history:
Received 16 October 2020
Received in revised form 28 January 2021
Accepted 30 January 2021
Available online 3 February 2021

Keywords:
Heparin
NMR
Electrostatic interaction
Antidote
Degradation

ABSTRACT

The highly anionic synthetic pentasaccharide fondaparinux (FDPX) – representing the antithrombin binding sequence of heparin – is in clinical use as a potent anticoagulant. Contrary to the unfractionated heparin, FDPX lacks potent antidote completely reversing its anticoagulant activity, therefore it is of great importance to identify new structures exhibiting strong intermolecular interactions towards FDPX. The polycationic heptakis(6-amino-6-deoxy)-beta-cyclodextrin (NH_2-β-CD) can serve as an excellent model compound to mimic these interactions between the oppositely charged oligosaccharides. Herein, extensive NMR spectroscopic and nano-electrospray ionization mass spectrometric (nESI-MS) studies were conducted to understand the molecular-level interactions in the FDPX - NH_2-β-CD systems. NMR experiments were performed at pD 7.4 and 2.0. Job's method of continuous variation and ^{1}H NMR titration experiments suggested the formation of FDPX·NH_2-β-CD complex at pD 7.4, while the presence of multiple complexes was assumed at pD 2.0. Stability constants were determined by separate ^{1}H NMR titrations, yielding log β_{11}=3.65 ± 0.02 at pD 7.4, while log $\beta_{11} \geq 4.9$ value suggested a high-affinity system at pD 2.0. 2D NOESY NMR studies indicated spatial proximities between the anomeric resonance α-L-iduronic acid residue and the cyclodextrin's methylene unit in the proximity of the cationic amino function. Acidic degradation of FDPX was investigated by NMR and MS for the first time in detail confirming that desulfation occurs involving one to two sulfate moieties. The desulfation of FDPX was inhibited by the cationic cyclodextrin in the case of equimolar ratio at pD 2.0. This is the first report on the stabilizing effect of cyclodextrin complexation on heparin degradation.

1. Introduction

Heparin is an anionic, linear polysaccharide, a member of the glycosaminoglycan (GAG) family that is naturally synthesized and stored in mast cells [1]. Although the core structure of heparin consists of repeating 1,4-linked uronic acid and glucosamine disaccharides, it has a microheterogenous and polydisperse structure due to various modification of the monosaccharide subunits. The hexuronic acid is either α-L-iduronic acid (IdoA) or β-D-glucuronic acid (GlcA), which may be 2-*O*-sulfated. The hexosamine residue is D-glucosamine (GlcN), which may be sulfated at the 3-*O* and 6-*O* positions and *N*-sulfated (GlcNS), *N*-acetylated (GlcNAc) or may be unmodified as a primary amine [2]. Heparin is best known for its anticoagulant activity, exerted through the interaction with the protease inhibitor antithrombin-III (AT-III). AT-III is the major plasma coagulation inhibitor, whose main targets are IIa and Xa activated coagulation factors [3]. Heparin is a widely used anticoagulant drug in the clinical practice despite its numerous undesirable side effects.

Nowadays, low molecular weight heparins (LMWHs) are applied in the clinical practice as an anticoagulant agent due to their predictable activity profile, better bioavailability and longer half-life, that contribute to their safer applicability. LMWHs are prepared from unfractionated heparin by chemical or enzymatic depolymerization reactions that produce polydisperse mixtures of heparin-derived oligosaccharides [4].

* Corresponding author.
E-mail address: beni.szabolcs@pharma.semmelweis-univ.hu (S. Béni).

https://doi.org/10.1016/j.jpba.2021.113947

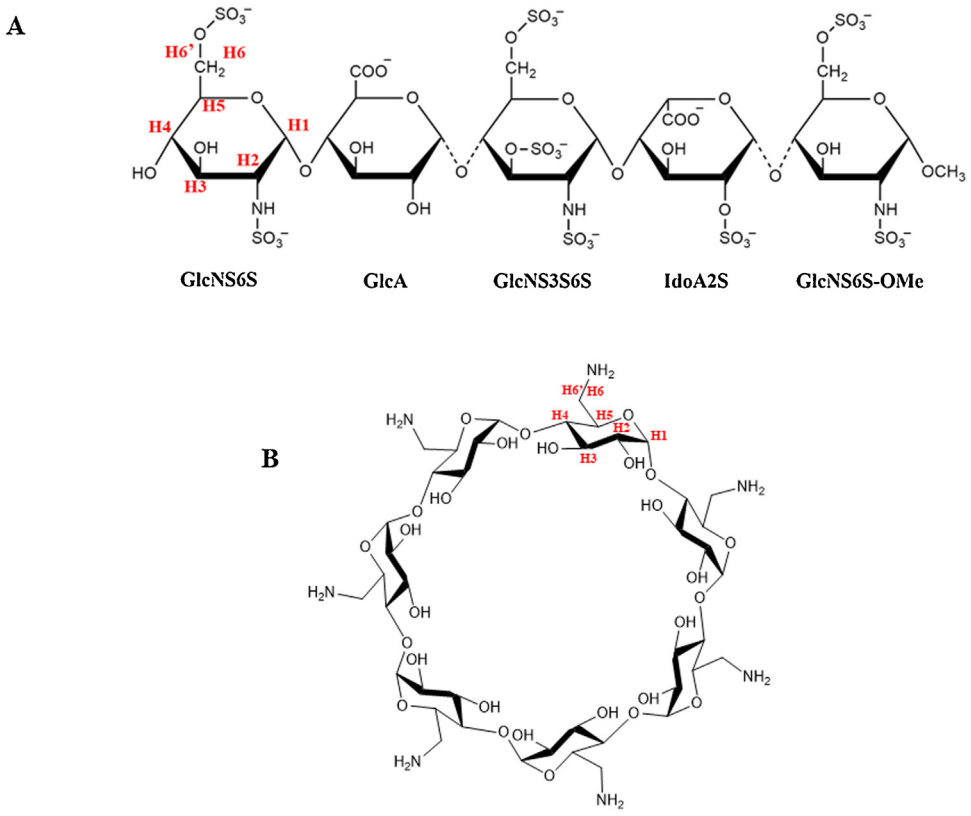

Fig. 1. Chemical structures and numbering of the fondaparinux (A) and the heptakis(6-amino-6-deoxy)-beta-cyclodextrin (B).

Another alternative in heparin-based anticoagulant therapy is the synthetic pentasaccharide fondaparinux (FDPX). It was designed to mimic the heparin pentasaccharide sequence present in each heparin derivative and required to bind AT-III, thus enhancing its inhibitory activity toward factor Xa [5]. FDPX is a methyl glucoside analogue of the heparin pentasaccharide sequence responsible for AT-III binding (Fig. 1). To neutralize the anticoagulant effect of heparin, protamine sulfate is usually used in the clinical practice. It is a basic, polycationic peptide isolated from salmon sperm, which binds to the polyanionic heparin through electrostatic interactions, thus forming an inactive complex without anticoagulant effect [6]. Unfortunately, protamine is unable to reverse the anticoagulant function of LMWHs and is even less effective for fondaparinux. Therefore, it is necessary to find new antidotes, which should be effective for all heparin derivatives [7]. Among the possible core structures as future antidotes, modified carbohydrates and cyclodextrins stand out as promising candidates [8].

Cyclodextrins are cyclic oligosaccharides built of D-glucopyranose units linked via α-1,4-glycosidic bonds. As a result, they have a truncated cone shape with a lipophilic inner cavity and a hydrophilic outer surface [9]. This particular structure enables reversible inclusion complex formation with guest molecules with appropriate properties [10]. Interactions between the cyclodextrin host and the guest molecules are generally noncovalent: hydrogen bonds, van der Waals and hydrophobic interactions are common, while in case of ionic derivatives electrostatic interactions dominate. The most commonly used native cyclodextrins are the α-, β- and γ-cyclodextrin composed of six, seven and eight glucose units, respectively. Synthetic modification of the hydroxyl groups of the glucopyranose units offers numerous possibilities for the preparation of various cyclodextrins, such as cationic and anionic derivatives. In the present study the cationic heptakis(6-amino-6-deoxy)-beta-cyclodextrin (NH_2-β-CD) was utilized (Fig. 1). These chemical modifications are often aimed at providing structure-specific interactions, thereby contributing to an even more pronounced supramolecular assembly [11,12].

The current study aims to characterize the molecular interactions between the polyanionic FDPX and the polycationic cyclodextrin NH_2-β-CD as a potential heparin antidote. Furthermore, the stabilizing effect of the NH_2-β-CD (hereinafter denoted as CD) on FDPX degradation under acidic conditions was also investigated. To establish a more profound understanding of the intermolecular interaction as well as the degradation of FDPX under acidic conditions, extensive NMR and MS experiments were performed.

2. Materials and methods

2.1. Chemicals and reagents

CD was a product of CycloLab Ltd. (Budapest, Hungary). D_2O (99.9 atom% D) was purchased from Merck (Darmstadt, Germany), while fondaparinux was isolated from Arixtra® 2.5 mg/0.5 mL injections. Briefly, ten prefilled injections were combined and subjected to dialysis (Spectra/Por® dialysis membrane – Biotech- CE Tubing MWCO: 100–500 Da) against deionized water for three consecutive days. Thereafter, the dialysate was subjected to freeze-drying. Other base chemicals of analytical grade were purchased from commercial suppliers and were used without further purification.

2.2. NMR spectroscopy

Nuclear magnetic resonance (NMR) spectroscopy measurements were carried out on a 600 MHz Varian DDR NMR spectrometer (Agilent Technologies, Palo Alto, CA, USA), equipped with a 5 mm inverse-detection probehead and gradient unit. Standard pulse sequences and processing routines available in VnmrJ

3.2C/Chempack 5.1 were used. The complete resonance assignments of the fondaparinux and the CD were established from direct $^{1}H–^{13}C$, long-range $^{1}H–^{13}C$, and scalar spin-spin connectivities derived from 1D ^{1}H, 2D ^{1}H-^{1}H gCOSY, zTOCSY (mixing time of 150 ms), ROESYAD (mixing time of 400 ms), NOESY and $^{1}H–^{13}C$ gHSQCAD (J =140 Hz – according to the one bond heteronuclear coupling constant) experiments. The ^{1}H chemical shifts were referenced to the methyl singlet (δ =3.31 ppm) of internal CH_3OH, a reference substance without any possible interaction with the CD.

Additional NMR studies were performed on an 800 MHz Bruker Avance III HDX800 MHz spectrometer equipped with a 5 mm $^{1}H/^{13}C/^{15}N$ Triple Resonance ^{13}C Enhanced Salt Tolerant Cold Probe (^{1}H: 799.7 MHz, ^{13}C: 201.0 MHz), controlled by the TopSpin 3.5 pl 7 software (Bruker Biospin GmbH, Rheinstetten, Germany). All NMR spectra were acquired in standard 5 mm NMR tubes at 25 °C.

2.2.1. ^{1}H NMR titration experiments

The stoichiometry of FDPX complexation with CD was investigated by the Job's method of continuous variation [13]. Samples were prepared in 0.1 M phosphate buffers of pD 2.0 and pD 7.4, at 25 °C temperature. The total molar concentration of the two components, c_{FDPX} + c_{CD} was kept constant at 3 mM, while the mole fraction of FDPX, $x_{FDPX} = c_{FDPX}/(c_{FDPX} + c_{CD})$ was varied gradually in 0.1 unit steps from 0 to 1. ^{1}H chemical shifts δ^{FDPX} were recorded at 600 MHz for several FDPX protons and complexation-induced displacement values, $\Delta\delta^{FDPX} = \left|\delta^{FDPX} - \delta_{FDPX}\right|$ were calculated with respect to δ_{FDPX} measured in the absence of CD. To construct Job's plots, $\Delta\delta^{FDPX}$ values were multiplied by the mole fraction of FDPX and depicted as a function of x_{FDPX}. Analogous plots were generated for selected protons of the CD.

Since the experimental design underlying Job's plots may not be optimal to determine the stability constants of the formed complexes [14], separate NMR titrations were performed under the same experimental conditions as used for the Job's plot. At pD 7.4, increasing portions ranging from 20 to 280 μL of 20.1 mM CD solution were added to 600 μL of 3.4 mM FDPX solution residing in the NMR tube. At pD 2.0, 600 μL of 3.18 mM FDPX solution was titrated with 10–250 μL of 20.9 mM CD stock solution. Following equilibration, ^{1}H NMR spectra were recorded in each titration step at 600 MHz and 25 °C temperature. The experimental titration curves for well-resolved resonances of FDPX and CD were evaluated by the OPIUM software [15] according to the principles summarized here by assuming the formation of both FDPX·CD and FDPX·2CD complexes as a general case. If complexation occurs with rapid kinetics on the NMR chemical shift timescale, the observed chemical shift $\delta^{FDPX,i}$ of any carbon-bound proton in FDPX becomes a mole-fraction weighted average [14] of the species-specific values in the uncomplexed FDPX (δ^{i}_{FDPX}) and those in the complexes ($\delta^{i}_{FDPX\cdot CD}$ and $\delta^{i}_{FDPX\cdot 2CD}$),

$$\delta^{FDPX,i} = \frac{[FDPX]\,\delta^{i}_{FDPX} + [FDPX\cdot CD]\,\delta^{i}_{FDPX\cdot CD} + [FDPX\cdot 2CD]\,\delta^{i}_{FDPX\cdot 2CD}}{c_{FDPX}} \quad (1)$$

where square brackets denote equilibrium concentrations and i used herein is a running index. Analogously defined intrinsic chemical shifts (δ^{j}_{CD}, $\delta^{j}_{FDPX\cdot CD}$, $\delta^{j}_{FDPX\cdot 2CD}$) and resonance signal averaging apply for any carbon-bound proton of the cyclodextrin:

$$\delta^{CD,j} = \frac{[CD]\,\delta^{j}_{CD} + [FDPX\cdot CD]\,\delta^{j}_{FDPX\cdot CD} + 2\,[FDPX\cdot 2CD]\,\delta^{j}_{FDPX\cdot 2CD}}{c_{CD}} \quad (2)$$

where square brackets denote equilibrium concentrations and j used herein is a running index. The mass-balance equations for both constituents read:

$$c_{FDPX} = [FDPX] + [FDPX\cdot CD] + [FDPX\cdot 2CD] \quad (3)$$

$$c_{CD} = [CD] + [FDPX\cdot CD] + 2\,[FDPX\cdot 2CD] \quad (4)$$

which can be reformulated in terms of the β association (i.e. binding or formation) constants of the complexes, yielding:

$$c_{FDPX} = [FDPX](1 + \beta_{11}\,[CD] + \beta_{12}[CD]^2) \quad (5)$$

$$c_{CD} = [CD](1 + \beta_{11}\,[FDPX] + 2\beta_{12}\,[FDPX]\,[CD]) \quad (6)$$

Based on the input values of c_{FDPX} and c_{CD} for each titration point (the ratio of which was checked from non-overlapping ^{1}H NMR integrals of the components) as well as initial guesses of the β stability constants, the OPIUM program solved the nonlinear system of Eqs. (5) and (6) for the variables [FDPX] and [CD]. These speciation calculations were integrated into a least-squares fitting procedure of Eqs. (1) or (2) to the measured dataset in order to iteratively refine the stability constant(s). Since the OPIUM program lacks a graphical output, the resulting equilibrium constants were used to compute species distribution data covering the 0–2.7 4 interval of the $\frac{c_{CD}}{c_{FDPX}}$ ratio by the ORCHESTRA program [16]. These datasets were subsequently imported into Microsoft Excel 2002, where Eqs. (1) and (2) were used to calculate and depict the continuous curves fitted to the experimental ^{1}H NMR titration datasets.

2.2.2. NMR structural studies on complex formation

To explore the spatial arrangement of the host-guest complexes and identify the interacting molecular sequences, nuclear Overhauser effect (NOE) type experiments were performed at c_{CD} = c_{FDPX} =1 mM in unbuffered samples at different pD values (2.0–7.4) to eliminate the possible interfering effect of the phosphate ions. NOE is a manifestation of dipolar cross relaxation between two nonequivalent nuclear spins that are close enough (<5 Å) through space [17]. The NOE intensities are scaled with r^{-6}, where r represents the mean distance between the protons. 2D NOESY spectra were acquired on the 600 MHz instrument, with mixing times of 400 ms using 16 scans on 1258 × 512 data points. For the acidic sample, 2D NOESY spectra were also recorded on the 800 MHz instrument, collecting 24 scans on 4096 × 512 data points, applying mixing times of 350 ms, 400 ms, 500 ms and 650 ms along with a 250-μW presaturation on the HDO signal for D1 = 2.5 s.

2.2.3. NMR investigations of FDPX degradation

To determine the structure of the FDPX decomposition product, ^{1}H and several 2D (COSY, TOCSY, HSQC, ROESY) NMR spectra were recorded at 600 MHz with the same parameters described in chapter 2.2. For this experiment, 5 mM FDPX was dissolved in a 0.1 M phosphate buffered D_2O at pD 2.0.

During the stability investigation, FDPX:CD samples with 1:0, 2:1 and 1:1 molar ratios were tested. All samples were dissolved in 0.1 M phosphate buffered D_2O at pD 2.0. In the case of the first set of experiments, ^{1}H NMR spectra of the freshly prepared samples were recorded. After keeping these samples at 25 °C for a week, their ^{1}H NMR spectra were recorded again. A second experiment was carried out to perform an accelerated decomposition investigation. ^{1}H NMR spectra of the fresh samples were recorded at 25 °C, then samples were incubated at 60 °C for 14 h. Afterwards all samples were cooled down to 25 °C again and ^{1}H spectra were re-recorded.

2.3. Electrospray ionization mass spectrometry

Mass spectrometric measurements were performed in negative ion mode on a modified Synapt G2-S HDMS Q-IMS-ToF hybrid mass spectrometer (Waters Co., Manchester, UK), equipped with a nanoelectrospray ion (nESI) source and an rf-confining drift cell (250.5 mm in length). An MKS 647C multichannel controller (MKS Instruments, Andover, Massachusetts, US) provided gas flow and pressure control in the drift cell, which was filled with He buffer gas (99.999% purity) at a pressure of 1.8 torr.

For studying the complex formation between FDPX and CD, the compounds were dissolved in water:methanol (50/50, v/v) to reach a concentration of 20 μM for FDPX and 200 μM for CD. The solvent mixture was prepared using Milli-Q® water and LC–MS grade methanol (Merck, Darmstadt, Germany). For MS experiments involving the FDPX degradation products, 5 mM FDPX was dissolved in a 0.1 M phosphate buffered D_2O at pD 2.0 and incubated at 60 °C for 14 h, identically to the solution used for NMR spectroscopic degradation measurements (see Section 2.2.3). This acidic solution was diluted in water:methanol (50/50) and spiked with a 10 mM aqueous solution of CD to reach a concentration of 20 μM for FDPX degradation products (calculated for the pre-incubation FDPX content) and 200 μM for CD.

For generating negative ions using nESI, 5 μL of the sample solutions described above was loaded into in-house prepared borosilicate needles coated with Pt/Pd (80/20), and a voltage of -0.60 to -0.85 kV was applied to the capillary. Typical instrument settings of the Synapt G2-S HDMS instrument were as follows: capillary voltage -0.60 to -0.85 kV; source temperature 100 °C; sampling cone 2.0; source offset 0.0; trap gas flow 2.0 mL min^{-1}; trap DC entrance 4.0; trap DC bias 2.0; trap DC −2.0; trap DC exit 1.0; IMS DC entrance −23.0; helium cell DC 55.0; IMS bias 45.0; helium exit −40.0; IMS DC exit 5.0; transfer DC entrance 5.0; transfer DC exit 15.0; trap wave velocity 250 m s^{-1}; trap wave height 0.8 V; transfer wave velocity 300 m s^{-1}; transfer wave height 4.0 V. All mass spectra were recorded in resolution mode. For clarity, polarities and units of the values above are provided as displayed in the MassLynx 4.1 software package (Waters Co., Manchester, UK). As such, some voltages are given only with numerical values with no unit specified.

Data processing and analysis were performed using MassLynx 4.1 (Waters Co., Manchester, UK) and Origin 2017 (OriginLab, Northampton, MA, US) software packages.

3. Results and discussion

3.1. Exploring the complex formation equilibria by NMR titrations

Intermolecular interactions between FDPX and CD were investigated at two different pD values (pD 2.0 and 7.4), where the charge distribution of the interacting species is different. At the physiological pD value, the CD derivative bears an average positive charge of 5.1 (pK_a values for the CD are as follows: 9.50(1), 8.89(1), 8.33(1), 8.07(1), 7.57(1), 7.35(1), 6.75(1) [18]), while at pD 2.0 the host is fully protonated, carrying seven positive charges. In the case of FDPX according to the published related oligosaccharides the pK_a values are 2.35 and 3.44 for β-D-GlcA and IdoA2S [19], thus at pD 7.4 both hexuronic acid residues are deprotonated, therefore FDPX possesses 10 negative charges. Under acidic conditions (pD 2.0), the mean charge of FDPX corresponds to −8.3. Complete ^{1}H NMR assignments of FDPX and CD at pD 2.0 and 7.4 can be found in Table S1 of Supporting Information.

In order to assess the complexation stoichiometry at pD 7.4, Job's plots were constructed from well-separated NMR signals of FDPX, such as those of the anomeric protons of the GlcNS6S, GlcA and GlcNS3S6S residues, the H1 and H5 resonances of IdoA2S, and the anomeric H1 resonance of the CD. All the Job's plot curves depicted on A and B diagrams in Fig. 2 show a maximum at x_{FDPX} = 0.5, suggesting the sole formation of the FDPX·CD complex with 1:1 stoichiometry.

During the subsequent single-tube NMR titration of FDPX with CD at the same pD value (see the stack plot in Fig. 3A), the chemical shift variation of the following protons with non-overlapping signals were monitored: GlcA H1, GlcNS3S6S H1, GlcNS6S-OMe H1, GlcNS3S6S H6, IdoA2S H5 and H1, GlcNS6S H1 of FDPX and H1 of the CD derivative. Titration profiles of the latter two nuclei are depicted in Fig. 3B, while those of the remaining FDPX protons listed above are shown in Fig. S1. All the eight datasets could be adequately fitted using the OPIUM program by assuming only the single FDPX·CD complex, as suggested by the Job's plots. These evaluations yielded estimates for the binding constant log β_{11} ranging from 3.25 to 4.3, collected in Table S2. In order to extract a more robust and reliable, single value of this stability constant [20], the eight datasets were subjected to simultaneous nonlinear regression using the same software. The quality of fit remained virtually the same for all the observed nuclei and this global evaluation yielded log β_{11} = 3.65 with an estimated standard deviation of 0.02, a moderately strong binding affinity for a CD complex (see the species distribution plot in Fig. S2). The complexation-induced changes in chemical shifts exceeded 0.04 ppm units for the GlcNS3S6S H5, IdoA2S H1 and H5 protons of FDPX, the intrinsic chemical shifts (listed in Table S3) emerging from the global data fitting only slightly differed from their counterparts from single-dataset evaluations in Table S2.

The Job's plots recorded at pD 2.0 revealed a less clear-cut picture about complexation (see Fig. 2, subplot C and D). While the profile of the anomeric CD proton in subplot D is rather wide but bears a maximum at x_{CD} = 0.5, suggesting again a simple 1:1 complexation pattern, the extremum of each FDPX proton's profile in Fig. 2, subplot C is consequently shifted to ca. x_{FDPX} = 0.6, indicating the presence of a 2FDPX·CD complex besides FDPX·CD.

To explore the complexation equilibria at pD 2.0 more thoroughly, a single-tube ^{1}H NMR titration of FDPX with the CD was carried out (see the stack plot in Fig. S3). Titration profiles of the anomeric protons belonging to the GlcNS6S and GlcNS3S6S units are depicted in Fig. 4, while those for four additional protons of FDPX as well as for the CD anomeric proton are shown in Fig. S4. Most titration profiles of FDPX protons consist of two quasi linear segments, with a minimal curvature near the crossing point at $c_{CD} = c_{FDPX}$. This type of titration curve is characteristic to a rather high-affinity system, for which merely the lower limit of the binding constant is accessible by curve-fitting [14]. The entire dataset cannot be fitted satisfyingly assuming the formation of a single FDPX·CD complex (see the blue curves in Fig. 4 and Fig. S4), the Hamilton's R factor, a goodness-of-fit criterion for the simultaneous fitting of the seven datasets, is 0.031%. The intrinsic chemical shifts are listed in Table S4. Hence the titration curves were evaluated in two steps.

All experimental datasets can be nicely fitted up to $\frac{c_{CD}}{c_{FDPX}} = 1$ with the assumption of a single FDPX·CD complex only (blue curves in Fig. 4 and Fig. S4), yielding log β_{11} = 4.9 ± 0.1, but higher values of this stability constant give virtually the same goodness-of-fit. Addition of a 2FDPX·CD species to the equilibrium model, as suggested by Job's plots, did not furnish a meaningful value for β_{21}, the iterations by the OPIUM program did not converge. Intuitively, one cannot describe the monotonic change in FDPX chemical shifts beyond the equimolar composition by the {FDPX·CD, 2FDPX·CD} equilibrium model. Instead, an FDPX·2CD complex was postulated besides FDPX·CD. A global fitting involving these two species was already able to describe the titration profiles of FDPX and CD protons in the full range of concentrations studied (see the fitted red curves in Figs. 4 and S4), the Hamilton's R factor decreased to 0.0089%, indicating a more appropriate equilibrium model. The calculations yielded a stability constant of log β_{12} = 8 for the FDPX·2CD complex (but this value again represents merely a lower limit). The intrinsic chemical shift values of species are collected in Table S5. Using these lower limits of the stability constants, the speciation curves in Fig. S5 were constructed for the concentration range explored in the NMR titration.

The discrepancy of Job's method and the chemical shift titration in establishing the correct stoichiometry of complexation is

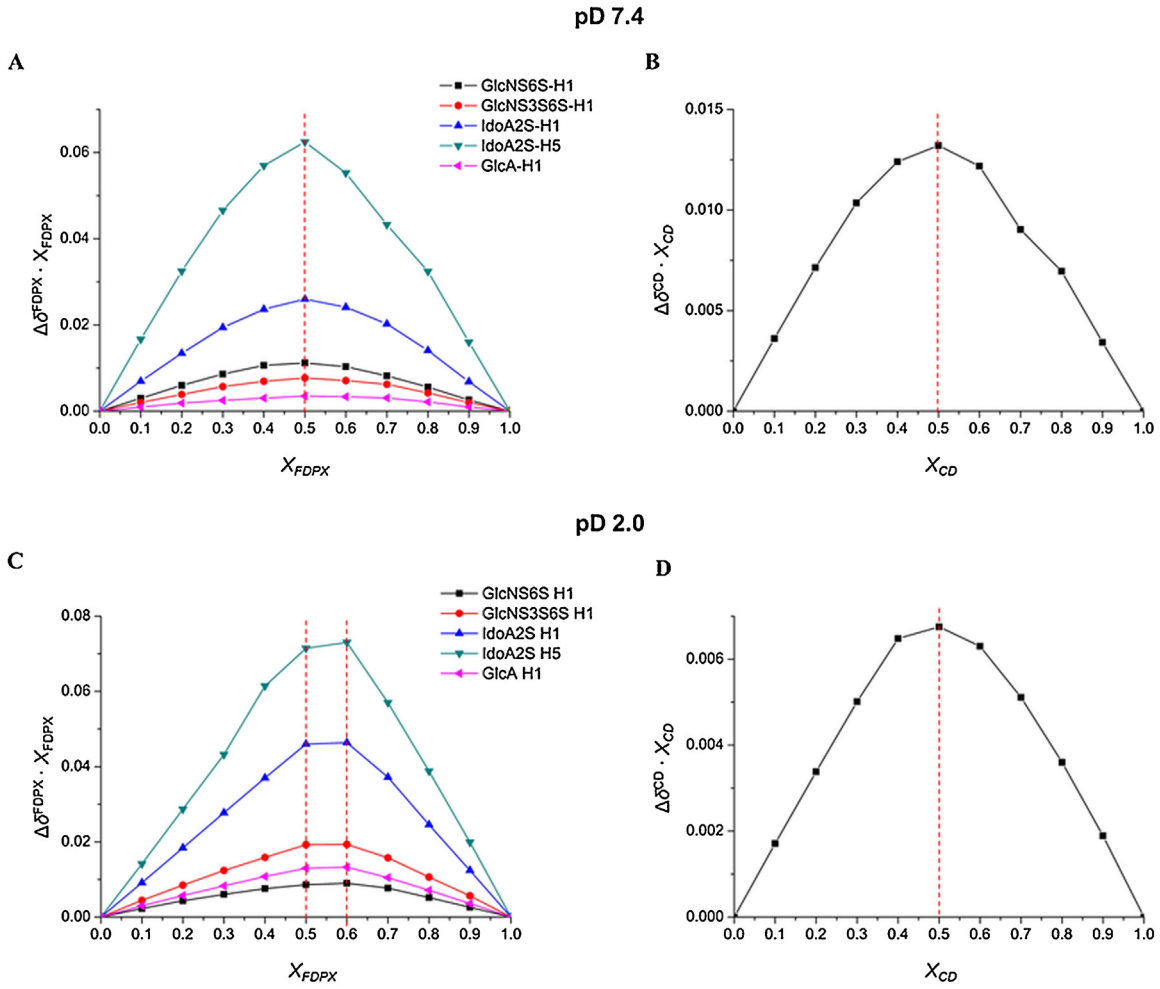

Fig. 2. Job's plot for the selected ^{1}H resonances of FDPX at pD 7.4 (**A**) and at pD 2.0 (**C**) and that of the anomeric resonance of NH_2-β-CD at pD 7.4 (B) and at pD 2.0 (D), respectively.

somewhat puzzling. Nevertheless, recent publications [21] [22] emphasize the limitations of Job's method of equilibrium systems beyond the simplest 1:1 case, being highly sensitive e.g. to the ratio of equilibrium constants [21]. While Job's method remains a reliable tool in stoichiometric studies of inorganic metal complexes, a careful inspection of the distribution of residuals of data-fitting [20,21] or the ranking of all reasonable binding models according to estimated uncertainties and other chemometric descriptors [22] became the recommended protocols for the same task in the field of supramolecular chemistry. Since the {FDPX·CD, FDPX·2CD} equilibrium model nicely reproduced the entire titration dataset, the formation of these two species can be regarded as most probable under the applied experimental conditions for this high-affinity system.

3.1.1. NMR structural studies

To obtain atomic-level information about the 3D structure of the FDPX-CD complex, NOE experiments were carried out for samples without phosphate buffer, to eliminate any possible interfering effect of the phosphate ions with the CD. Solutions at pD 2.0–7.4 were tested. The 2D NOESY spectrum for all pD values revealed that the H6 protons of the CD give intermolecular contacts with the FDPX's IdoA2S H1 proton – as shown in Fig. 5 for the pD 2.0 sample. NOE experiments were performed at several FDPX:CD molar ratios, however, none of the experiments confirmed dipolar correlations between the inner protons of the CD and FDPX. Hence only outer-sphere, electrostatics-driven complex formation can occur between these oligosaccharides as also found in a recent study [23].

3.1.2. NMR investigations of FDPX degradation

It is well known from the literature, that sulfated polysaccharides can undergo degradation (depolymerization and desulfation) under acidic conditions. However, there are no detailed studies that provide relevant information on FDPX. Recording the ^{1}H NMR spectra of aqueous FDPX sample at pD 2.0 after a week of storage indicated that new ^{1}H resonances appeared, see Fig. 6. In order to identify the structure of the degradation product, additional 2D spectra were recorded. The spin system of the monosaccharide subunits of the degradation product was identified by COSY and TOCSY experiments, respectively. ^{1}H–^{13}C HSQC experiment evidenced that the anomeric carbon of the GlcNS3S6S unit ($\Delta\delta$ =6 ppm) and the C5 resonance of the IdoA2S moiety ($\Delta\delta$ = 2 ppm) exhibited remarkable shifts compared to the intact FDPX (Fig. S6). A 2D ROESY experiment (Fig. S7) was performed to establish the connectivity of the monosaccharides. Based on the ROESY data the pentasaccharide chain remained intact during the applied circumstances of degradation. Therefore, the observed chemical shift changes upon decomposition (Fig. S8) cannot be attributed to the depolymerization of the FDPX backbone. Consequently, as supported by earlier studies on the acid hydrolysis of sulfated polysaccharides [24], sulfate loss of FDPX occurred in our case. Seto et al. followed the chemical shift changes in heparin undergoing desulfation by ^{1}H

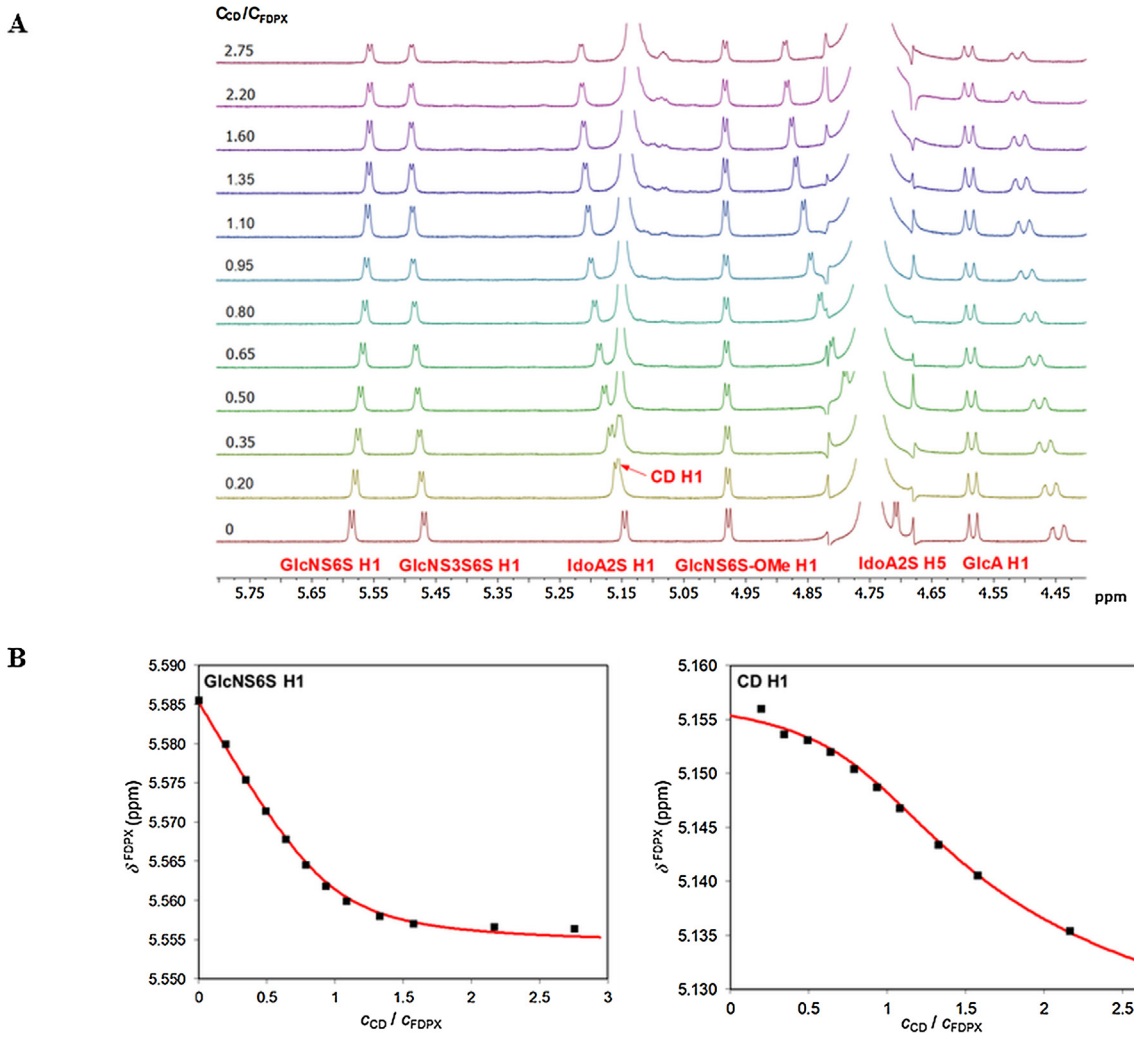

Fig. 3. Representative ^{1}H NMR chemical shift changes (subplot A) of the FDPX ^{1}H resonances upon titration of 3.4 mM FDPX solution with increasing portions of a 20.1 mM NH_2-β-CD solution at pD 7.4. Titration profiles of FDPX GlcNS6S H1 and GlcNS3S6S H1 nuclei (subplot B) at pD 7.4, fitted by the 1:1 complexation model using the OPIUM program (red curves).

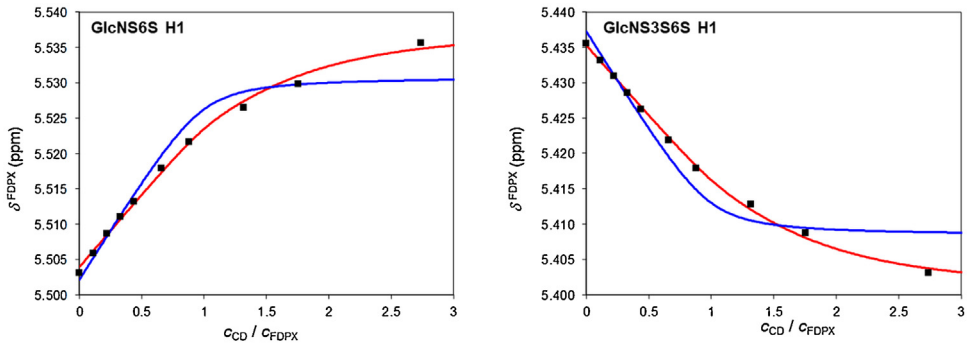

Fig. 4. Titration profiles of the anomeric protons of the FDPX GlcNS6S and GlcNS3S6S units at pD 2.0. Blue curves were fitted by the 1:1 complexation model, while a global fitting assuming the FDPX·CD and the FDPX·2CD species are shown by red curves.

NMR measurements [25]. Their result also supports our data, as desulfation leads to downfield shift of particular resonances. The largest ^{1}H NMR chemical shifts changes were observed in the case of the IdoA2S and the trisulfated (GlcNS3S6S) subunits (Fig. S8), suggesting that the sulfate loss primarily affected these units. Further investigations were conducted to support this hypothesis by mass spectrometry.

To overcome the unwanted desulfation of FDPX in solution, the possible protective function of CD was explored. To demonstrate the stabilizing effect of the CD, ^{1}H NMR spectra of the freshly prepared pD 2.0 samples with 1:0, 2:1 and 1:1 (FDPX:CD) molar ratios were recorded. All samples were incubated at 25 °C for a week, then ^{1}H NMR spectra were re-recorded. As shown in Fig. 6, almost 50% of the FDPX degraded in the absence of CD. The decomposition process slowed down significantly in the presence of half

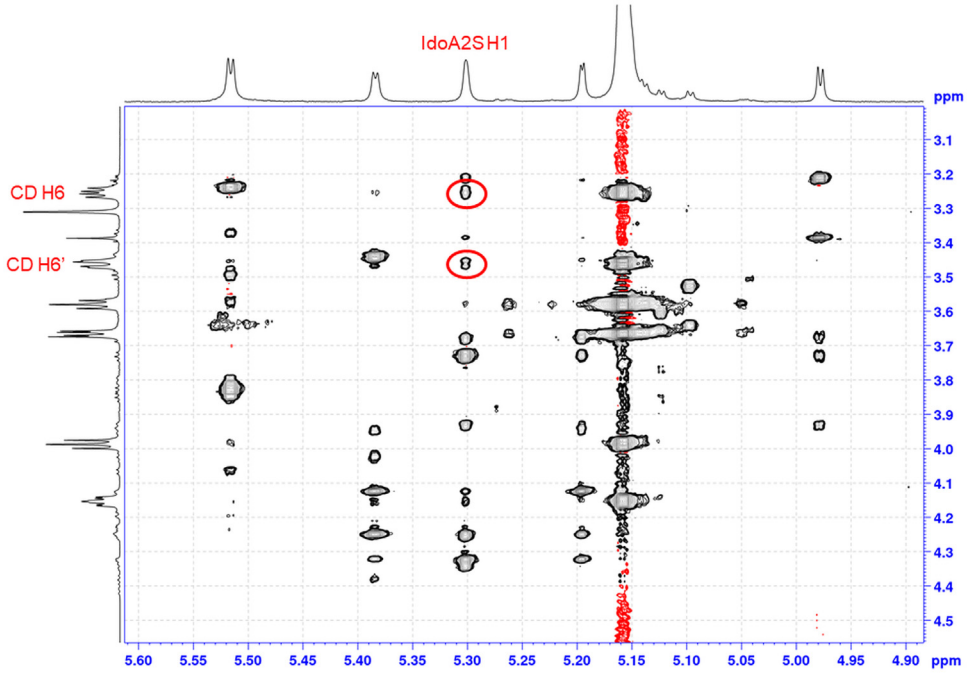

Fig. 5. Partial 2D ROESY NMR spectra of a pD 2.0 sample containing FDPX and CD at 1:1 molar ratio, showing cross-peaks between the IdoA2S H1 proton and the CD H6 resonance.

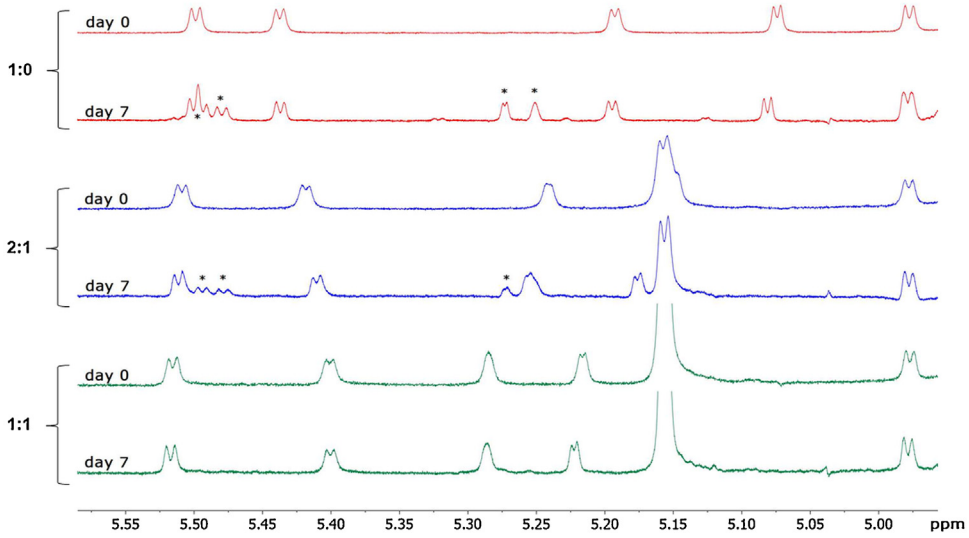

Fig. 6. The ^{1}H NMR spectra of the freshly prepared FDPX:CD samples (day 0) and that of the same samples stored at 25 °C for a week (day 7) at different molar ratios (red 1:0, blue 2:1, green 1:1) under pD 2.0 conditions. The ^{1}H resonances of the decomposition product are indicated by *.

equivalent CD, as only 20% degradation could be observed by ^{1}H NMR. However, samples of equimolar FDPX and CD however revealed no detectable degradation of FDPX. Applying even higher molar ratios of CD, complete protection of FDPX was observed, therefore, a minimum of equimolar CD is necessary to prevent desulfation.

To accelerate the decomposition of FDPX, samples with the same molar ratios were incubated at 60 °C for 14 h. ^{1}H NMR spectra were registered prior and after the incubation at room temperature (Fig. S9). The sample without CD degraded completely, while those containing CD exhibited less pronounced desulfation. In the presence of 1:1 molar ratio minor degradation could be observed, while molar excess of CD (1:2 molar ratio) completely hindered the desulfation.

3.2. Studying FDPX degradation by nESI-MS

To study the complex formation between FDPX and CD by MS-based methods, the compounds were dissolved in a water:methanol mixture (50/50, v/v) at a concentration of 20 μM for FDPX and 200 μM for CD, yielding a 1:10 molar ratio. A representative mass spectrum obtained in negative ion mode is shown in Fig. 7a (non-informative parts of the spectrum outside the *m*/*z* range of 400–1400 were omitted for clarity). No signal corresponding to unbound FDPX could be detected, and the spectrum is dominated by mass peaks of singly- and doubly-charged CD ions, as well as by triply- and quadruply-charged FDPX·CD complexes displaying exclusively 1:1 stoichiometry. The assignment of species along with *m*/*z* values reflecting monoisotopic masses are given in

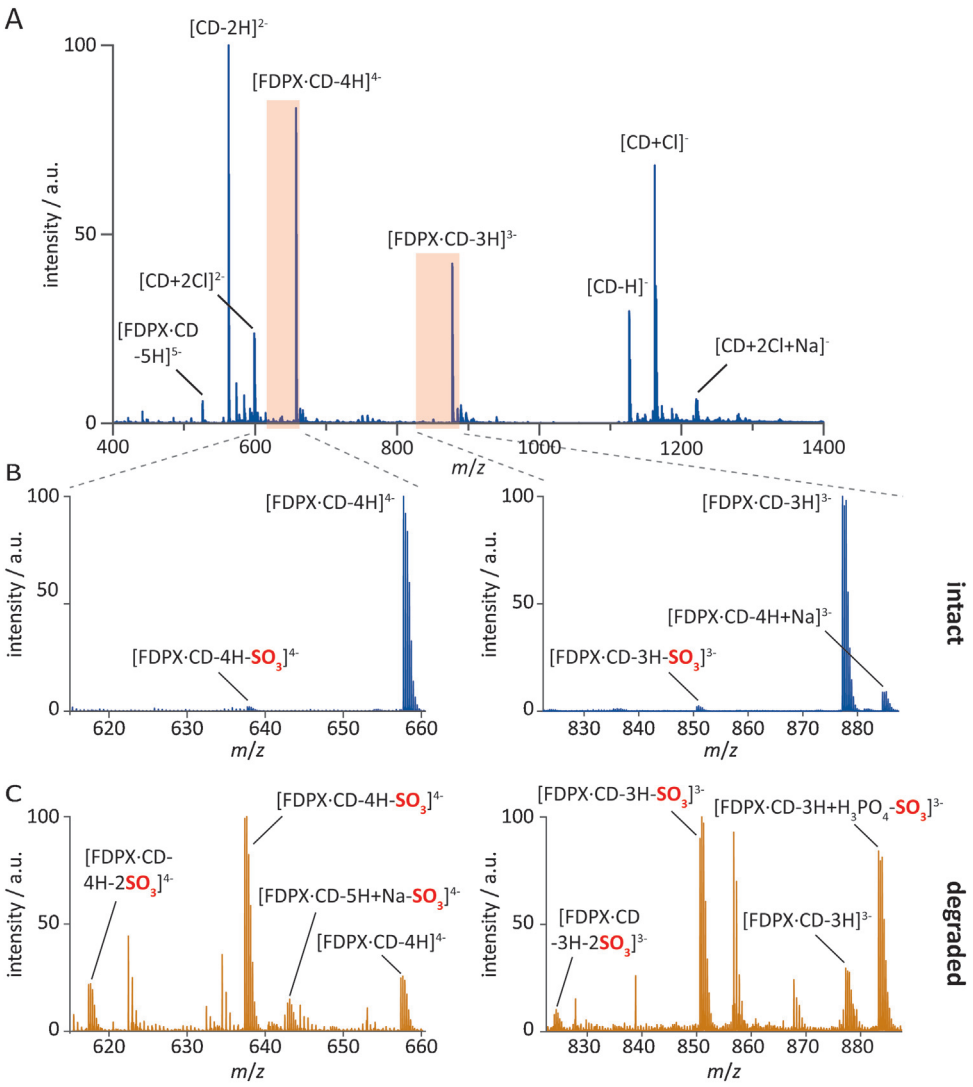

Fig. 7. Complex formation of fondaparinux and its degradation product with per-6-amino-β-cyclodextrin studied by nano-electrospray ionization mass spectrometry. (A) Negative ion mode nESI mass spectrum of a solution containing 20 μM fondaparinux (FDPX) and 200 μM per-6-amino-β-cyclodextrin (CD). Unbound CD ions and corresponding mass peaks: $[CD+2Cl + Na]^-$ at *m/z* 1220.41; $[CD + Cl]^-$ at *m/z* 1162.45; $[CD-H]^-$ at *m/z* 1126.47; $[CD+2Cl]^{2-}$ at *m/z* 598.71 and $[CD-2 H]^{2-}$ at *m/z* 562.73. CD:FDPX complex ions and respective mass peaks: $[FDPX·CD-3 H]^{3-}$ at *m/z* 877.14; $[FDPX·CD-4 H]^{4-}$ at *m/z* 657.6 and $[FDPX·CD-5 H]^{5-}$ at *m/z* 525.88. (B) Insets highlighting diagnostic parts of the full mass spectrum shown at the top. The low extent of sulfate loss in the presence of CD is apparent: the intensity of mass peaks corresponding to $[FDPX·CD-3H-SO_3]^{3-}$ at *m/z* 850.48 and $[FDPX·CD-4H-SO_3]^{4-}$ at *m/z* 637.61 are roughly two orders of magnitude lower than those of the respective intact species. (C) Diagnostic parts of negative ion mode nESI mass spectra of a solution containing fondaparinux degradation products (20 μM), spiked with 200 μM CD. Dominant species with one to two sulfate losses and the respective mass peaks: $[FDPX·CD-3H+H_3PO_4-SO_3]^{3-}$ at *m/z* 883.14; $[FDPX·CD-3H-SO_3]^{3-}$ at *m/z* 850.48; $[FDPX·CD-3H-2SO_3]^{3-}$ at *m/z* 823.83; $[FDPX·CD-5H + Na-SO_3]^{4-}$ at *m/z* 643.11; $[CD·FDPX-4H-SO_3]^{4-}$ at *m/z* 637.61 and $[FDPX·CD-4H-2SO_3]^{4-}$ at *m/z* 617.62. Other major peaks not assigned in the figure correspond to deprotonated CD ions of lower charge states (forming adducts with various numbers of H_3PO_4 and Na^+), bearing no relevance to the degradation in question. All *m/z* values given above reflect monoisotopic masses.

the figure caption. The findings are in agreement with NMR spectroscopic results, allowing for the confident determination of the FDPX·CD complex stoichiometry based on orthogonal analytical methods.

In general, highly-sulfated glycosaminoglycan (GAG) ions are rather fragile in the gas phase: the loss of neutral SO_3 (79.96 Da) upon ion heating in the source or during collision induced dissociation is a dominant dissociation channel in MS-based experiments, posing a major difficulty in the analysis of heparin and related species [26–28]. Interestingly, the FDPX·CD complex remains predominantly intact upon transfer from solution to the gas phase. This effect is analogous to the prevention of sulfate equivalent losses by pairing highly-sulfated GAGs with basic arginine-rich peptides in MS experiments [29,30]. When electrospraying a solution of FDPX in the presence of excess quantities of CD, little sulfate loss is observed as shown exemplarily in Fig. 7b. The peaks corresponding to $[FDPX·CD-3H-SO_3]^{3-}$ and $[FDPX·CD-4H-SO_3]^{4-}$ are weak, with intensities below 5% of those of the respective intact complexes. The appearance of these minor peaks in the mass spectrum can be explained by two, mutually non-exclusive processes. Most probably, some loss of neutral SO_3 occurs from the intact $[FDPX·CD-3H]^{3-}$ and $[FDPX·CD-4H]^{4-}$ ions during the MS experiment. The other possibility is that partially degraded FDPX is already present in solution, forming a complex with the cyclodextrin.

The stabilizing effect exerted by CD on the sulfate groups of FDPX not only facilitated the analysis of the intact FDPX·CD complex, but also proved to be highly advantageous for the structural characterization of the fondaparinux degradation products.

MS experiments were used to monitor the sulfate loss in FDPX upon incubation in acidic media. For these degradation measure-

ments samples were incubated as described in Section 2.3. Briefly, a phosphate buffered pD 2.0 solution of 5 mM FDPX was incubated at 60 °C for 14 h, diluted in water:methanol (50/50, v/v), then spiked with the cationic cyclodextrin to reach a concentration of 20 μM for the FDPX degradation products (calculated for the pre-degradation FDPX content) and 200 μM for CD. Under experimental conditions identical to those applied to record the spectrum displayed in Fig. 7a and b (blue trace), markedly different mass spectra were obtained for the sample containing FDPX degradation products, as highlighted in Fig. 7c (yellow trace). Owing to potential differences in the ionization/ion transmission efficiency of the various species, exact quantitative information may not be extracted from the MS experiments. However, the dominance of mass peaks corresponding to FDPX-related ions with sulfate losses, such as $[FDPX{\cdot}CD\text{-}3H{+}H_3PO_4\text{-}SO_3]^{3-}$, $[FDPX{\cdot}CD\text{-}3H\text{-}SO_3]^{3-}$, $[FDPX{\cdot}CD\text{-}3H\text{-}2SO_3]^{3-}$, $[FDPX{\cdot}CD\text{-}5H + Na\text{-}SO_3]^{4-}$, $[FDPX{\cdot}CD\text{-}4H\text{-}SO_3]^{4-}$ and $[FDPX{\cdot}CD\text{-}4H\text{-}2SO_3]^{4-}$, is clearly visible in the spectra in Fig. 7c. Combining these results with the finding that CD complexation efficiently hinders neutral loss of SO_3 from FDPX in the gas phase, we can conclude that the mass spectra reflect the composition of the solution and the distribution of species therein. That is, the intense signals corresponding to the ions listed above are not artefacts caused by gas-phase SO_3 loss during the MS experiment, but instead correspond to degradation products already present in solution.

In conclusion, results of MS experiments support NMR spectroscopic findings, enabling the unambiguous assignment of the FDPX·CD complex stoichiometry. In addition, utilizing the beneficial stabilizing effect of CD-complexation on the sulfate groups of FDPX in the gas phase, MS provides evidence that the degradation products of FDPX are pentasaccharides with an intact glycan backbone, displaying predominantly one, and to a lesser extent two sulfate losses.

4. Conclusions

In the present study, the intermolecular interactions of fondaparinux with heptakis(6-amino-6-deoxy)-beta-cyclodextrin were characterized extensively by NMR spectroscopy in solution and by nESI-MS in the gas phase. NMR spectroscopic studies revealed 1:1 stoichiometry and moderate affinity ($\log \beta_{11} = 3.65 \pm 0.02$) at pD 7.4, while at pD 2.0 thermodynamically more stable species were deduced: FDPX·CD ($\log \beta_{11} \geq 4.9 \pm 0.1$) and FDPX·2CD ($\log \beta_{12} \geq 8$). The possible interaction site involving the IdoA2S moiety and the cationic part of the cyclodextrin has also been localized based on 2D NMR studies. An in-depth characterization of the acidic degradation of FDPX by NMR and MS experiments suggested desulfation of the pentasaccharide backbone at pD 2.0. Under these conditions, the heptacationic cyclodextrin successfully prevents sulfate loss by strong electrostatic interactions. Thus, our findings contribute to a better understanding of heparin stabilization under acidic conditions, offering an efficient method to prevent the unwanted decomposition of heparinoids.

CRediT authorship contribution statement

Bianka Várnai: Formal analysis, Investigation, Writing - original draft, Writing - review & editing, Visualization. **Márkó Grabarics:** Investigation, Writing - original draft, Writing - review & editing, Visualization. **Zoltán Szakács:** Methodology, Formal analysis, Writing - review & editing, Visualization. **Kevin Pagel:** Resources, Writing - review & editing, Funding acquisition. **Milo Malanga:** Investigation, Writing - review & editing. **Tamás Sohajda:** Resources, Writing - review & editing, Funding acquisition.

Declaration of Competing Interest

The authors declare that they have no known competing financial interests or personal relationships that could have appeared to influence the work reported in this paper.

Acknowledgments

S.B. thanks the financial support from the János Bolyai Research Scholarship of the Hungarian Academy of Sciences and from the Bolyai + New National Excellence Program of the Ministry of Human Capacities (ÚNKP-20-5-SE-31). M.G. and K.P. gratefully acknowledge financial support from the Freie Universität Berlin, the Max Planck Society and the German Research Foundation under grant number FOR2177/P03. M.M. and T.S are grateful for the support of the Hungarian National Research, Development and Innovation Office (OTKAK-125093).

Thanks are due to Prof. Csaba Szántay Jr. for his support of the 800 MHz NMR measurements at Gedeon Richter Plc.

Appendix A. Supplementary data

Supplementary material related to this article can be found, in the online version, at doi:https://doi.org/10.1016/j.jpba.2021.113947.

References

[1] R.J. Linhardt, 2003 Claude S. Hudson award address in carbohydrate chemistry. Heparin: structure and activity, J. Med. Chem. 46 (2003) 2551–2564, http://dx.doi.org/10.1021/jm030176m.
[2] C.J. Jones, S. Beni, J.F.K. Limtiaco, D.J. Langeslay, C.K. Larive, Heparin characterization: challenges and solutions, Annu. Rev. Anal. Chem. 4 (2011) 439–465, http://dx.doi.org/10.1146/annurev-anchem-061010-113911.
[3] B. Mulloy, J. Hogwood, E. Gray, R. Lever, C.P. Page, Pharmacology of heparin and related drugs, Pharmacol. Rev. 68 (2015) 76–141, http://dx.doi.org/10.1124/pr.115.011247.
[4] E. Gray, B. Mulloy, T.W. Barrowcliffe, Heparin and low-molecular-weight heparin, Thromb. Haemost. 99 (2008) 807–818, http://dx.doi.org/10.1160/TH08-01-0032.
[5] H. Naimy, N. Leymarie, M.J. Bowman, J. Zaia, Characterization of heparin oligosaccharides binding specifically to antithrombin III using mass spectrometry, Biochemistry 47 (2008) 3155–3161, http://dx.doi.org/10.1021/bi702043e.
[6] M. Schroeder, J. Hogwood, E. Gray, B. Mulloy, A.M. Hackett, K.B. Johansen, Protamine neutralisation of low molecular weight heparins and their oligosaccharide components, Anal. Bioanal. Chem. 399 (2011) 763–771, http://dx.doi.org/10.1007/s00216-010-4220-8.
[7] M.A. Crowther, L.R. Berry, P.T. Monagle, A.K.C. Chan, Mechanisms responsible for the failure of protamine to inactivate low-molecular-weight heparin, Br. J. Haematol. 116 (2002) 178–186, http://dx.doi.org/10.1046/j.1365-2141.2002.03233.x.
[8] B. Kalaska, K. Kaminski, E. Sokolowska, D. Czaplicki, M. Kujdowicz, K. Stalinska, J. Bereta, K. Szczubialka, D. Pawlak, M. Nowakowska, A. Mogielnicki, Nonclinical evaluation of novel cationically modified polysaccharide antidotes for unfractionated heparin, PLoS One 10 (2015) 1–21, http://dx.doi.org/10.1371/journal.pone.0119486.
[9] L. Szente, J. Szemán, Cyclodextrins in analytical chemistry: host-guest type molecular recognition, Anal. Chem. 85 (2013) 8024–8030, http://dx.doi.org/10.1021/ac400639y.
[10] L. Liu, Q.X. Guo, The driving forces in the inclusion complexation of cyclodextrins, J. Incl. Phenom. Macrocycl. Chem. 42 (2002) 1–14, http://dx.doi.org/10.1023/A:1014520830813.
[11] S. Hbaieb, R. Kalfat, Y. Chevalier, N. Amdouni, H. Parrot-Lopez, Influence of the substitution of β-cyclodextrins by cationic groups on the complexation of organic anions, Mater. Sci. Eng. C 28 (2008) 697–704, http://dx.doi.org/10.1016/j.msec.2007.10.013.
[12] F. D'Anna, S. Riela, P. Lo Meo, M. Gruttadauria, R. Noto, The binary pyrene/heptakis-(6-amino-6-deoxy)-β-cyclodextrin complex: a suitable chiral discriminator. Spectrofluorimetric study of the effect of some α-amino acids and esters on the stability of the binary complex, Tetrahedron Asymmetry 13 (2002) 1755–1760, http://dx.doi.org/10.1016/S0957-4166(02)00418-4.
[13] P. Job, Formation and stability of inorganic complexes in solution, Ann. Chim. (Paris) 9 (1928) 113–203.
[14] L. Fielding, Determination of association constants (K(a)) from solution NMR data, Tetrahedron 56 (2000) 6151–6170, http://dx.doi.org/10.1016/S0040-4020(00)00492-0.

[15] Solution Equilibria Analysis with the OPIUM Computer Program, The full version of the OPIUM program is available (free of charge) at http://web.natur.cuni.cz/~kyvala/opium.html (accessed on 19. September, 2020).
[16] J.C.L. Meeussen, Orchestra: an object-oriented framework for implementing chemical equilibrium models, Environ. Sci. Technol. 37 (2003) 1175–1182, http://dx.doi.org/10.1021/es025597s, The full version of the ORCHESTRA program is available (free of charge) at http://orchestra.meeussen.nl/ (accessed on 19. September, 2020).
[17] D. Neuhaus, M.P. Williamson, The Nuclear Overhauser Effect in Structural and Conformational Analysis, 2nd ed., Wiley-VCH, 2000.
[18] G. Wenz, C. Strassnig, C. Thiele, A. Engelke, B. Morgenstern, K. Hegetschweiler, Recognition of ionic guests by ionic β-cyclodextrin derivatives, Chem. - A Eur. J. 14 (2008) 7202–7211, http://dx.doi.org/10.1002/chem.200800295.
[19] H.M. Wang, D. Loganathan, R.J. Linhardt, Determination of the pK(a) of glucuronic acid and the carboxy groups of heparin by 13C-nuclear-magnetic-resonance spectroscopy, Biochem. J. 278 (1991) 689–695, http://dx.doi.org/10.1042/bj2780689.
[20] W. Al-Soufi, P.R. Cabrer, A. Jover, R.M. Budal, J.V. Tato, Determination of second-order association constants by global analysis of 1H and 13C NMR chemical shifts, Steroids 68 (2003) 43–53, http://dx.doi.org/10.1016/s0039-128x(02)00114-9.
[21] F. Ulatowski, K. Dabrowa, T. Bałakier, J. Jurczak, Recognizing the limited applicability of job plots in studying host-guest interactions in supramolecular chemistry, J. Org. Chem. 81 (2016) 1746–1756, http://dx.doi.org/10.1021/acs.joc.5b02909.
[22] D. Brynn Hibbert, P. Thordarson, The death of the Job plot, transparency, open science and online tools, uncertainty estimation methods and other developments in supramolecular chemistry data analysis, Chem. Commun. (Camb.) 52 (2016) 12792–12805, http://dx.doi.org/10.1039/c6cc03888c.
[23] S.J. Berners-Price, A.K. Gorle, T. Haselhorst, S.J. Katner, A. V Everest-Dass, D. James, E.J. Peterson, J.E. Koblinski, K. Takabe, M. Von Itzstein, P. Nicholas, Angenwandte Chemie, (n.d.). https://doi.org/10.1002/anie.202013749.
[24] A. Kalsson, S.K. Singh, Acid hydrolysis of sulphated polysaccharides. Desulphation and the effect on molecular mass, Carbohydr. Polym. 38 (1999) 7–15, http://dx.doi.org/10.1016/s0144-8617(98)00085-x.
[25] S.P. Seto, T. Miller, J.S. Temenoff, Effect of selective heparin desulfation on preservation of bone morphogenetic protein-2 bioactivity after thermal stress, Bioconjug. Chem. 26 (2015) 286–293, http://dx.doi.org/10.1021/bc500565x.
[26] M.J. Kailemia, L. Li, M. Ly, R.J. Linhardt, I.J. Amster, Complete mass spectral characterization of a synthetic ultralow-molecular- weight heparin using collision-induced dissociation, Anal. Chem. 84 (2012) 5475–5478, http://dx.doi.org/10.1021/ac3015824.
[27] R. Huang, C. Zong, A. Venot, Y. Chiu, D. Zhou, G.J. Boons, J.S. Sharp, De novo sequencing of complex mixtures of heparan sulfate oligosaccharides, Anal. Chem. 88 (2016) 5299–5307, http://dx.doi.org/10.1021/acs.analchem.6b00519.
[28] R.L. Miller, S.E. Guimond, R. Schwörer, O.V. Zubkova, P.C. Tyler, Y. Xu, J. Liu, P. Chopra, G.J. Boons, M. Grabarics, C. Manz, J. Hofmann, N.G. Karlsson, J.E. Turnbull, W.B. Struwe, K. Pagel, Shotgun ion mobility mass spectrometry sequencing of heparan sulfate saccharides, Nat. Commun. 11 (2020) 1–12, http://dx.doi.org/10.1038/s41467-020-15284-y.
[29] G. Venkataraman, Z. Shriver, R. Raman, R. Sasisekharan sequencing complex polysaccharides, Science 286 (1999) 537–542, http://dx.doi.org/10.1126/science.286.5439.537.
[30] J. Zaia, Glycosaminoglycan glycomics using mass spectrometry, Mol. Cell Proteomics 12 (2013) 885–892, http://dx.doi.org/10.1074/mcp.R112.026294.